

**Continuous-variable quantum key distribution under strong channel polarization disturbance**Wenyuan Liu , Yanxia Cao, Xuyang Wang, and Yongmin Li *State Key Laboratory of Quantum Optics and Quantum Optics Devices, Institute of Opto-Electronics, Shanxi University, Taiyuan 030006, People's Republic of China**and Collaborative Innovation Center of Extreme Optics, Shanxi University, Taiyuan 030006, People's Republic of China*

(Received 20 February 2020; accepted 2 September 2020; published 25 September 2020)

In a commercial fiber-based quantum key distribution (QKD) system, the state of polarization (SOP) of the optical fields is inevitably disturbed by random birefringence of the standard single-mode fiber due to an external complex environment. We analyze theoretically the effect of SOP fluctuations on the continuous-variable (CV) QKD system and experimentally verify its validity. To overcome the influence of the polarization variations, a self-adaptive gradient algorithm is proposed to achieve high-speed polarization controlling under pulsed light with field programmable gate array hardware. For single random polarization scrambling, the polarization extinction ratio achieved is over 30 dB and the average time of polarization control is 827  $\mu$ s. In order to eliminate further the effect of the occasional failures of polarization control, we properly filter the raw keys in terms of the relative phase fluctuations between the signal and the local oscillator. By combining this approach with the high-speed polarization control, we demonstrate a CV QKD under a continuous polarization scrambling of 314 rad/s. Our results provide useful references for practical application of fiber-based CV QKD in a field environment.

DOI: [10.1103/PhysRevA.102.032625](https://doi.org/10.1103/PhysRevA.102.032625)**I. INTRODUCTION**

Quantum key distribution (QKD) guarantees unconditionally secure key sharing between two users (Alice and Bob) connecting through a quantum channel and an authenticated classical channel [1–6]. Its security depends on the primary principles of quantum mechanics rather than some kind of difficult mathematic problem. The enciphered message using the shared secure keys with a one-time pad protocol cannot be eavesdropped in principle by any third party (Eve) even though powerful quantum computing is employed. A number of QKD protocols have been successfully demonstrated using fiber links and free-space links in recent years and close to wide commercial applications. The continuous-variable (CV) QKD protocol has attracted much interest [7–29] because of its potential high secure key rate at medium and short distances, as well as good compatibility with passive optical communication networks [20,30–34].

The information-theoretic security of CV QKD has been proved strictly. Before its wide commercial applications, several challenges should be tackled; one of them is the practical security. For instance, imperfect real-world devices and a complex external environment may degrade the performance of the protocol and even lead to potential security threats [35–47]. In fiber-based CV QKD systems, one of the major impacts of the external environment is that the state of polarization (SOP) of the transmitted quantum signal field can be dramatically disturbed by elusive birefringence variations of the single-mode fiber. In this case, the signal field cannot interfere efficiently and stably with the local oscillator (LO)

and the output signals of the homodyne (heterodyne) detection will suffer from large fluctuations. On the other hand, the LO is usually polarization and time multiplexed with the quantum signal and both propagate through the same single-mode fiber. The fluctuations of the SOP will result in the mutual crosstalk between the LO and signal light. In reality, a typical time-multiplexing technique can provide isolation of about 80 dB, which is not enough to eliminate the leakage of the LO to the signal due to the strong LO pulse (around  $10^8$  photons/pulse). The crosstalk from the strong LO to signal can induce noise photons on the signal mode and increase the excess noise of the system. Furthermore, the fluctuation of the SOP of the signal results in an effective loss for the signal mode at the receiver due to the polarization demultiplexing. Therefore, the rapid fluctuations of the SOP can significantly deteriorate the performance of the CV QKD.

To counteract the adverse effect of polarization variations, dynamic polarization control methods which are able to convert arbitrarily the SOP to a target SOP are required [48–54]. For fiber-based discrete-variable QKD, some measures that track and rehabilitate the SOP impairments induced by the unpredictable birefringence effect of the long fiber have been demonstrated [55–60]. Those techniques include time-division (wavelength-division) multiplexing of strong reference and weak signal pulses, a polarization-basis tracking scheme using revealed sifted key bits, and so on. Recently, an algorithm-based SOP prediction was reported in a local LO CV QKD system [61].

In this paper we investigate in detail the influence of SOP fluctuations on the CV QKD system and verify its validity in experiment. A self-adaptive gradient algorithm is developed to achieve field programmable gate array (FPGA) hardware-based high-speed polarization controlling under the pulsed

\*yongmin@sxu.edu.cn

light. With this technique, the polarization fluctuations of both the signal field and LO are effectively suppressed with a polarization extinction ratio (PER) over 30 dB and the average polarization recovering time reaches the submillisecond level (827  $\mu$ s) for a single random polarization scrambling. By using the high-speed self-adaptive gradient algorithm and properly handling the occasional failures of polarization control, we implement a CV QKD over a 50-km fiber channel under continuous polarization scrambling of 314 rad/s.

This paper is organized as follows. In Sec. II we investigate theoretically and experimentally the influence of the polarization variation of the signal and LO fields on the key parameters of the CV QKD system. In Sec. III we present a self-adaptive gradient algorithm to realize the high-speed SOP control and apply it to the CV QKD system under strong SOP disturbance. We summarize in Sec. IV.

## II. INFLUENCE MECHANISM OF SOP FLUCTUATIONS ON THE CV QKD SYSTEM

In this section we study the impact of the fluctuations of the SOP on the channel transmittance and channel excess noise of the CV QKD system.

### A. Channel parameters

First we assume that the receiver Bob recovers perfectly the initial SOP of the signal and LO. The output of Bob's time-domain balanced homodyne detector (BHD) is proportional to the quadrature component of the pulsed signal light, which is given by

$$\hat{V}_{\text{peak}} = |\alpha_l| \hat{X}_\theta, \quad (1)$$

where  $|\alpha_l|^2 = I_l$  is the average intensity of the LO,  $\hat{X}_\theta = \hat{a}_s e^{-i\theta} + \hat{a}_s^\dagger e^{i\theta}$  is the quadrature component of the signal light,  $\hat{a}_s$  denotes the annihilation operator of the signal light, and  $\theta$  is the relative phase difference between the signal light and LO. The normalized quadrature components of the signal light  $x_B$  and its variance  $V_B$  are written, respectively, as

$$x_B = \frac{\hat{V}_{\text{peak}}}{\sqrt{N_0}} = \hat{X}_\theta, \quad (2)$$

$$V_B = V(\hat{X}_\theta), \quad (3)$$

where  $N_0 = I_l$  is the shot noise. Based on Alice's and Bob's data, we can infer the channel transmittance  $T_0$  and excess noise  $\varepsilon_0$  of the QKD system [14,43]

$$T_0 = \frac{\langle x_A x_B \rangle^2}{\eta \langle x_A^2 \rangle^2}, \quad (4)$$

$$\varepsilon_0 = \frac{V_B - 1 - v_{\text{ele}}}{\eta T_0} - V_A, \quad (5)$$

where  $x_A$  represents Alice's Gaussian data,  $V_A$  is Alice's modulation variance in shot noise units (SNU), and  $v_{\text{ele}}$  and  $\eta$  are the electronic noise and detection efficiency of the BHD detector, respectively.

Next we assume that the recovered PER at Bob's site is imperfect. Then the output of the BHD is rewritten as

$$\hat{V}'_{\text{peak}} = |\alpha'_l| \hat{X}'_\theta, \quad (6)$$

where  $|\alpha'_l|^2 = I'_l$  is the LO intensity and the shot noise becomes  $N'_0 = I'_l$ . In this case, we have

$$x'_B = \frac{\hat{V}'_{\text{peak}}}{\sqrt{N'_0}} = \hat{X}'_\theta, \quad (7)$$

$$V'_B = \frac{V(\hat{V}'_{\text{peak}})}{N'_0} = V(\hat{X}'_\theta). \quad (8)$$

As mentioned above, the imperfectly recovered PER at Bob's site leads to the signal loss and crosstalk from the LO to the signal light, i.e., a small portion of the LO photons is transferred to the signal mode. Considering that the signal light is at single-photon level and very weak, we ignore the effect of leakage from the signal light to the LO on the LO mode. The resulting LO  $\hat{a}'_l$  and signal field  $\hat{a}'_s$  are given by

$$\hat{a}'_l \approx \sqrt{(1-h)} |\alpha_l| e^{i\theta}, \quad (9)$$

$$\hat{a}'_s = \sqrt{(1-h)} \hat{a}_s + \sqrt{h} (\sqrt{q} |\alpha_l| e^{i\varphi} + \delta \hat{a}_V), \quad (10)$$

where  $\delta \hat{a}_V$  denotes the vacuum fluctuation of the LO field. The extinction ratio of the pulsed LO is  $q$  [62],  $\varphi$  is the relative phase between leaked LO photons and the signal light, and  $\bar{h} = 10^{-R/10}$  is the attenuation coefficient of the signal light due to the finite PER, where  $R$  is the recovered PER in Bob's site. Combining Eqs. (7)–(10), we have

$$x'_B = \sqrt{1-h} \hat{X}_\theta + \sqrt{h} \hat{X}_V + 2\sqrt{hq} |\alpha_l| \cos \varphi, \quad (11)$$

$$V(x'_B) = (1-h)V(X_\theta) + \bar{h} + 4\langle n_e \rangle (\cos \varphi)^2, \quad (12)$$

where  $\hat{X}_V$  is the quadrature component of the vacuum field. In addition,  $\langle n_e \rangle$  is the leaked average photon number from the LO to the signal mode, which satisfies  $\langle n_e \rangle = pq\bar{h}$ , where  $p$  is the average photon number per LO pulse at the receiver Bob.

Due to the degradation of the PER, the estimated  $T'_0$  and  $\varepsilon'_0$  differ from the original values of  $T_0$  and  $\varepsilon_0$ , which can be obtained using Eqs. (4) and (5) by substituting  $x'_B$ ,  $V(x'_B)$ , and  $v_{\text{ele}}$  for  $x_B$ ,  $V(x_B)$ , and  $v_{\text{ele}}/(1-h)$ , respectively. So  $T'_0$  and  $\varepsilon'_0$  can be expressed as

$$T'_0 = \frac{\langle x_A x'_B \rangle^2}{\eta \langle x_A^2 \rangle^2} = T_0(1-\bar{h}) \quad \text{and} \quad (13)$$

$$\varepsilon'_0 = \varepsilon_0 + \frac{4\langle n_e \rangle (\cos \varphi)^2 + \bar{h}}{\eta(1-\bar{h})T_0} + \frac{(1+v_{\text{ele}})(1-\frac{1}{1-\bar{h}})}{\eta T_0}. \quad (14)$$

From Eqs. (13) and (14) it is easy to verify that  $T'_0 \leq T_0$  and  $\varepsilon'_0 \geq \varepsilon_0$ . That means the performance of the QKD system is deteriorated due to the imperfect recovered PER.

### B. Experimental results

In this section we verify the above theoretical predictions in experiment. The experimental schematic is shown in Fig. 1. A 1550-nm continuous-wave single-frequency laser is chopped into optical pulses with a repetition rate of 500 kHz and pulse width of 100 ns using two Mach-Zehnder (MZ) intensity modulators (AM1); the optical pulses are successively split into a weak signal light and an intense LO by an asymmetric beam splitter. The signal light was Gaussian modulated in the phase space ( $\hat{X}_0, \hat{X}_{\pi/2}$ ) with a MZ intensity modulator (AM2) and a phase modulator (PM1). Then time-division multiplexing and

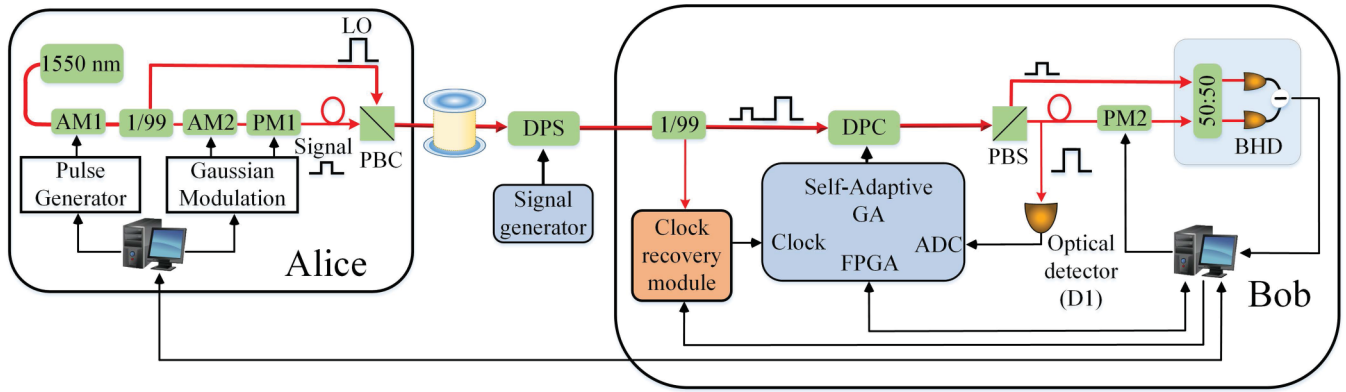


FIG. 1. Schematic diagram of the CV QKD system: AM, MZ amplitude modulator; PM, phase modulator; PBC, polarizing beam combiner; DPC, dynamic polarizing controller; DPS, dynamic polarizing scrambler; PBS, polarizing beam splitter; BHD, balanced homodyne detector; clock, external clock port on the FPGA; Self-Adaptive GA, self-adaptive gradient algorithm; DIO, digital input output; ADC, analog to digital converter.

polarization multiplexing approach is exploited to deliver the signal and LO to Bob's site by a 50-km single-mode optical fiber. Next Bob's site conducts polarization demultiplexing of the received signal light and the LO using a dynamic polarization controlling unit. By randomly switching the basis through altering the relative phase between the LO and signal light ( $0$  or  $\pi/2$ ), one of the two conjugate quadrature components of the signal light is measured. Finally, an authenticated classical channel between the sender Alice and the receiver Bob is used to implement the channel parameter estimation and data postprocessing.

The dynamic polarization controlling unit is composed of a polarization beam splitter (PBS), an optical detector, an FPGA hardware-based self-adaptive gradient algorithm, and a dynamic polarization controller. Here we use the fiber-squeezer-based dynamic polarization controller (DPC) for the advantage of lower insertion loss and fast response time. Because the laboratory environment is relatively stable, the PER at the output port of the PBS can stay at a constant value for a relatively long time (1 h). By controlling the DPC, we adjust the PER at the receiver to 30, 27, 25, 23, and 20 dB, respectively. For each PER point, we record the corresponding channel transmittance and excess noise of the QKD system, which are estimated in an interval of 20 min [43], or, more precisely, once every 2 min and repeated ten times.

Figure 2 shows the measured channel transmittance and excess noise as a function of the PER. The relevant experimental parameters are  $V_A = 5.6$ ,  $v_{\text{ele}} = 0.066$ , and  $\eta = 0.68$ . It is obvious that the evaluated excess noise increases with the decreasing PER, while the evaluated channel transmittance decreases as the PER decreases. This is because the imperfect polarization control causes signal light loss and crosstalk from the strong LO to the signal mode. In order to ensure the security of the QKD, we attribute these effects to the eavesdropping behaviors. Therefore, a lower PER will result in worse performance of the QKD system. As a comparison, the theoretical predictions are also plotted in Fig. 2 using Eqs. (13) and (14). The experimental results are in good agreement with the theoretical predictions.

From Eq. (13) it is clear that the decline of channel transmittance mainly depends on the loss of the signal mode. To

investigate the respective contributions of the crosstalk (leakage from the LO to the signal) and the signal mode loss to the excess noise, we simulate the excess noise  $\epsilon'_0$  at  $I_L = 0$ , which means that no leakage from the LO occurs. We find that the resulting excess noise  $\epsilon'_0$  is approximately equal to  $\epsilon_0$  under a different PER. Therefore, we can conclude that the crosstalk (leakage from the LO to the signal) is the dominant factor inducing the increase of excess noise.

### III. SELF-ADAPTIVE GRADIENT ALGORITHM

To overcome the adverse impact of the SOP fluctuations on the QKD, we propose a self-adaptive gradient algorithm to implement high-speed polarization control in real time. To this end, we divide the whole SOP on the Poincaré sphere into five regions according to the PER, which depend on the detected voltage signal  $V_{\text{out}}$  of the optical detector (D1) and have values of  $0 \leq V_{\text{out}} < 1$  V,  $1 \text{ V} \leq V_{\text{out}} < 2$  V,  $2 \text{ V} \leq V_{\text{out}} < 3$  V,  $3 \text{ V} \leq V_{\text{out}} < 4$  V, and  $4 \text{ V} \leq V_{\text{out}}$ , respectively. Notice that  $V_{\text{out}} = 4.2$  V corresponds to perfect polarization recovery. For each region on the Poincaré sphere, a set of

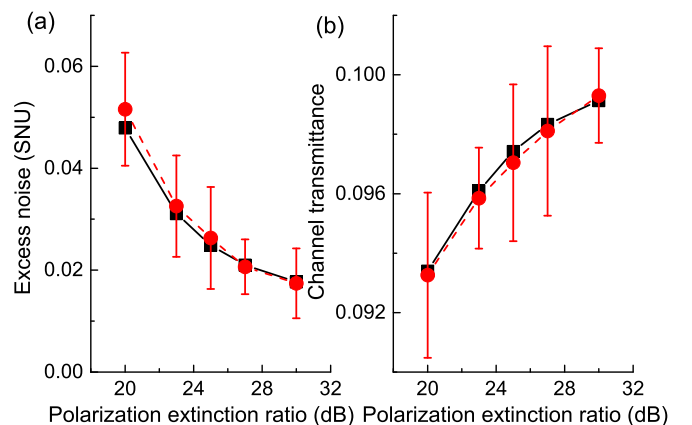


FIG. 2. Excess noise and channel transmittance versus different PERs: (a) excess noise and (b) channel transmittance. The red circles and black squares represent the experimental data and the theoretical simulation, respectively.

optimal parameters ( $k, d$ ) including the gradient  $k$  and step size  $d$  is sought for the gradient algorithm, and in total five sets of parameters are employed for the gradient algorithm. During the SOP control, the gradient algorithm automatically switches to the corresponding operation parameters according to the real-time monitored PER. By using this self-adaptive gradient algorithm, the total iterations of the algorithm are reduced significantly. If  $k > 0$ , the above iteration is repeated until the maximum value of the objective function (output voltage signal of the optical detector) is found, otherwise finding the minimum value. In our experiment,  $k$  is positive and the maximum value is sought. The procedures of the algorithm includes four stages, which are described as follows.

1. The output voltage of the optical detector  $V_{\text{out}}$  is acquired after the initial voltage  $V_1$  is loaded onto the the first stage of the DPC.

2. According to the value of  $V_{\text{out}}$ , a specific set of parameters ( $k, d$ ) is selected from the five sets of parameters to calculate the new voltage  $V'_1 = V_1 + d_1$ , where  $d_1$  represents the dithering voltage. The voltage  $V'_1$  is then loaded onto the DPC and the output of the optical detector is changed to  $V'_{\text{out}}$ .

3. Based on the above-obtained voltage values, the updated voltage loading onto the DPC is inferred as  $V''_1 = V'_1 + k_1(V'_{\text{out}} - V_{\text{out}})/d_1$ .

4. The second, third, and fourth stages of the DPC repeat steps 1–3 in turn. After the fourth stage finishes steps 1–3, the first stage restarts the next loop of iterations sequentially.

5. The entire program will abort until either of two conditions is satisfied: The PER reaches the desired target value or the iteration time is longer than its upper limit. In our system, the target value of the PER and the threshold iteration times are set to 30 dB and 36 times, respectively.

As depicted in Fig. 1, at Bob's site, a beam splitter (90:10) is used to split a small portion of the beam to recover the clock signal of the system. The signal light and LO are polarization demultiplexed by a dynamic polarization controller and a PBS. Part of the LO pulse is detected by an integral optical detector and the resulting peak voltage of the electric pulse output from the detector is acquired by the analog to digital converter on the FPGA as the feedback signal. By utilizing the FPGA hardware, the self-adaptive gradient algorithm can be quickly implemented to search for the target SOP and achieve high-speed polarization control under the pulsed light.

To test the performance of the polarization control unit, we randomly scramble the SOP on the Poincaré sphere by using the DPC and successively operate the polarization control unit to restore the SOP. Figure 3 illustrates the statistical analysis results for the probability of the recovered PER above 30 dB as a function of the consumed time of single-polarization control. The average time of the polarization control is less than 1 ms ( $827 \mu\text{s}$ ) and the overall probability of a recovered PER greater than 30 dB is 92%. There are some cases in which the recovered PER is less than 30 dB even though the iteration times of the self-adaptive gradient algorithm reach the upper limit.

Figure 4 shows a typical evolution process of the PER as a function of the iteration time under the condition of random single-polarization scrambling. We can see that the PER exhibits a nonlinear dependence on the iteration times. It rises rapidly with the increasing number of iterations at the initial

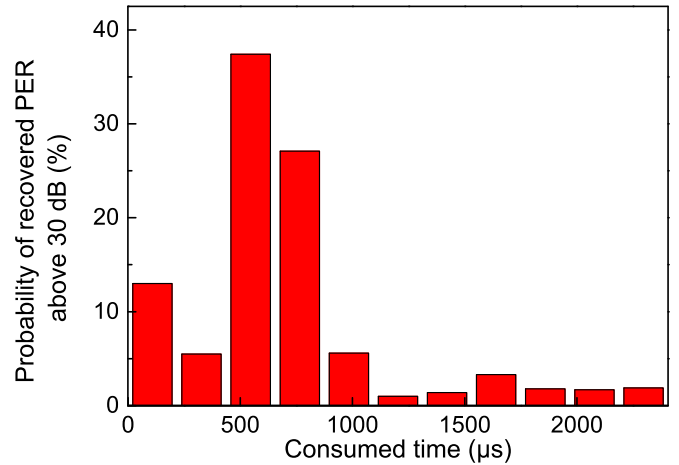


FIG. 3. Probability of the recovered PER above 30 dB versus the consumed time of single polarization control.

stage and reaches a flat region after about 15 iterations. After this point, the PER approaches saturation and starts to fluctuate around 30 dB even if more iteration times are applied. In terms of this phenomenon, a threshold decision (30 dB) is introduced in the gradient algorithm to effectively reduce the iterations and improve the efficiency of the polarization control.

By analyzing the time consumption of the polarization control unit, we find that the majority of time is spent acquiring the feedback voltage. In our current system, the sampling rate is 500 kS/s, which is limited by the repetition rate of the signal pulse. By improving the repetition rate to 50 MS/s, the total acquisition time of the polarization control unit may decrease from  $40 \mu\text{s}$  to  $400 \text{ ns}$  readily. The second factor is the response time of the dynamic polarization controller, which is around  $30 \mu\text{s}$  and can be improved to a level of  $100 \text{ ns}$  by using a lithium niobate waveguide-based dynamic polarization controller instead of the fiber-squeezer-based one used here. The third factor is the computation time of the algorithm, which is efficiently implemented by using FPGA

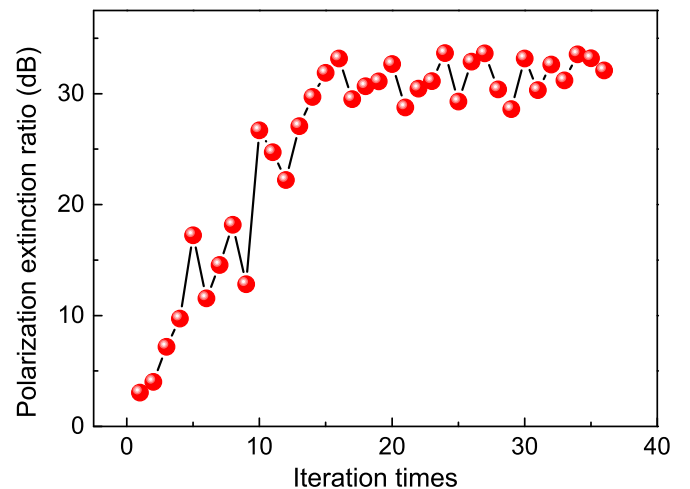


FIG. 4. Observed PER versus the iteration times for a typical single random polarization control.

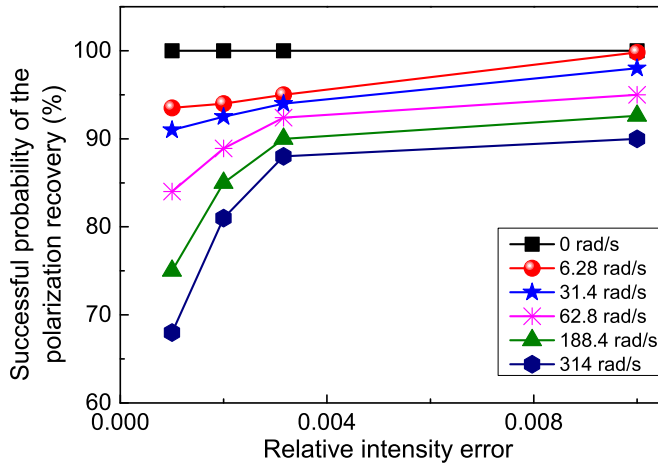


FIG. 5. Successful probability of the polarization recovery versus the relative intensity error under different continuous polarization scrambling rates.

hardware in our system. Further optimization of the algorithm and suppression of the computation time are possible.

Above we have analyzed the response characteristics of the polarization control unit under the conditions of random single-polarization scrambling. In the field environment, the external disturbance of the SOP is generally in a continuous manner. In the following, we utilize the DPC to continuously disturb the quantum channel to simulate the effect of field environments on the SOP.

As shown in Fig. 5, for different polarization scrambling rates of 6.28, 31.4, 62.8, 188.4, and 314 rad/s, we record and analyze the successful probability of polarization recovery versus the relative intensity error (RIE) [54]; here the RIE is defined as  $10^{-R/10}$ , with  $R$  the PER. For each curve corresponding to a specific polarization scrambling rate, the RIE is recorded at an interval of 2 ms and the total measurement time is 100 s. When there is no polarization scrambling, the measured RIE is smaller than 0.001. As the polarization scrambling rate gradually increases, the RIE increases accordingly. The successful probability of an observed RIE less than 0.0033 is higher than 90% when the polarization scrambling rate is as high as 62.8 rad/s.

Figure 6 shows the mean RIE as a function of polarization scrambling rate. We can see that the mean RIE remains almost unchanged and lower than 0.002 when the polarization scrambling rate is less than 100 rad/s. When the polarization disturbance increases further, the effect of the polarization control degrades obviously. The mean RIE increases to around 0.01 for a continuous scrambling rate of 314 rad/s.

#### IV. CV QKD UNDER STRONG CHANNEL POLARIZATION DISTURBANCE

In this section we apply the developed dynamic polarization controlling technique to the CV QKD system (Fig. 1) and investigate the performance of the system under strong polarization disturbance. As in Sec. II, the DPC is employed to simulate the impact of the field environment on the SOP. Under this condition, we investigate the characteristics of the

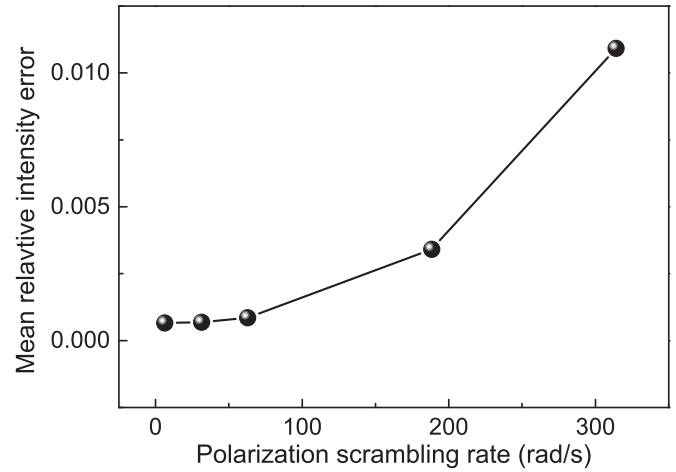


FIG. 6. Mean RIE versus different polarization scrambling rates.

key parameters of the CV QKD system, namely, the excess noise and channel transmittance.

We note that there is still a small probability that the SOP cannot be recovered well when the polarization control unit is activated and connected to the QKD system, and the corresponding RIE can be on the order of 0.1. In this scenario, although these failures occupy only a very small portion of the whole event, they can significantly disturb the locking of the relative phase between the signal and LO, which further affects the accurate estimation of both the excess noise and channel transmittance. Considering that the failure of the polarization control is closely related to the poor phase locking, in order to eliminate the effect of the occasional failures of polarization control, we propose to discard those raw keys for which the corresponding relative phase fluctuation is larger than a certain filtering threshold, as shown in Figs. 7 and 8.

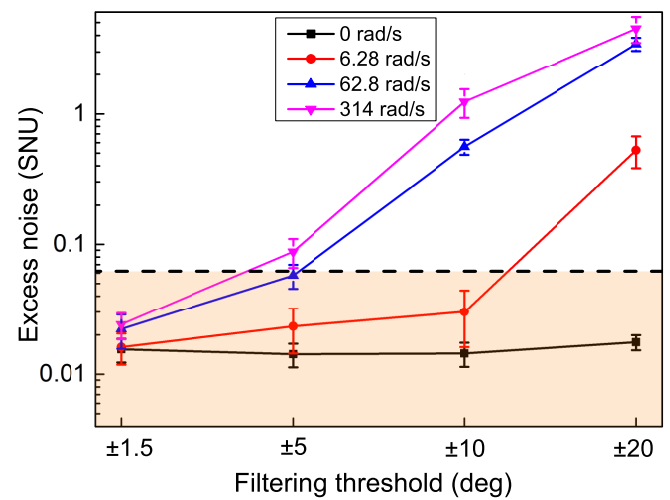


FIG. 7. Excess noise of the CV QKD system versus the filtering threshold of the relative phase fluctuations (peak to peak value) under different polarization scrambling rates. The dashed line denotes the excess noise level corresponding to the null secret key rate (the finite key effect is considered). The other experimental parameters are  $V_A = 5.6$ ,  $T_0 = 0.095$ ,  $v_{\text{ele}} = 0.066$ ,  $\eta = 0.68$ , and  $\beta = 95\%$ .

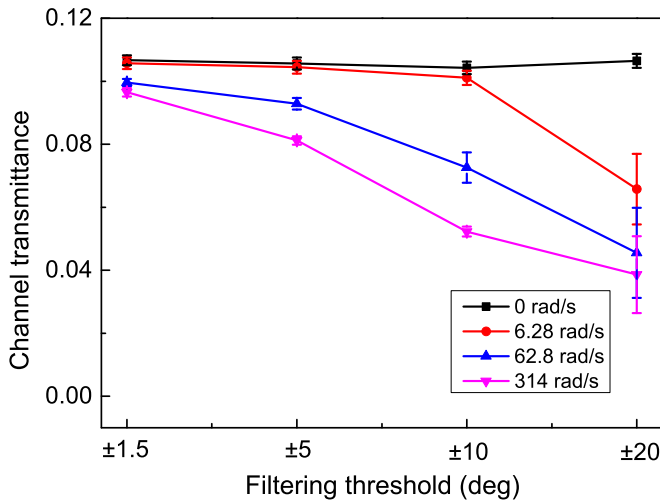


FIG. 8. Channel transmittance of the CV QKD system versus the filtering threshold of the relative phase fluctuations (peak to peak value) under different polarization scrambling rates.

Figures 7 and 8 depict the evaluated excess noise and channel transmittance of the CV QKD system as a function of the filtering threshold of relative phase fluctuations (peak to peak value) under different polarization scrambling rates. More precisely, at each polarization scrambling rate, we filter the raw Gaussian data and keep only those data whose relative phase fluctuations are lower than certain thresholds ( $\pm 1.5^\circ$ ,  $\pm 5^\circ$ ,  $\pm 10^\circ$ , and  $\pm 20^\circ$ ). In this way, we obtain four sets of raw keys and each set of raw keys is then used to evaluate the excess noise and channel transmittance of the system.

As shown in Figs. 7 and 8, when no polarization scrambling is applied (0 rad/s), the evaluated excess noise and channel transmittance are almost unchanged regardless of the threshold of the relative phase filtering. This is because the relative phase fluctuation can be well stabilized within  $\pm 1.5^\circ$ , which makes the filtering have a negligible effect on the raw data. With the increasing polarization scrambling, the relative phase fluctuation cannot be stabilized accurately and the filtering begins to take effect; the evaluated parameters vary explicitly with the threshold of the relative phase filtering. We can find that low filtering thresholds lead to lower excess noises and higher channel transmittance, which are beneficial to the QKD system.

At a polarization scrambling rate of 314 rad/s, given that the threshold of the relative phase fluctuation is set to  $\pm 20^\circ$ ,

the estimated excess noise will increase from the initial 0.015 to around 4 and the evaluated channel transmittance will decrease from the initial 0.096 to 0.038. In this case, the performance of the QKD system is seriously deteriorated and no secret key can be distilled (Fig. 7). By limiting the maximum value of the relative phase fluctuations to  $\pm 1.5^\circ$ , the change of the estimated excess noise and channel transmittance reduces significantly regardless of the different polarization scrambling. This measure, together with the high-speed polarization control algorithm, effectively overcomes the adverse impact of the polarization disturbance. The QKD system can still provide a positive secure key rate of 0.005 bit/pulse despite its quantum channel suffering from a polarization disturbance of 314 rad/s. Here the block length of the raw key is 75M samples and the finite key effect is considered [63].

## V. CONCLUSION

In summary, we have theoretically investigated and experimentally verified the impact of rapid fluctuations of the SOP on the CV QKD. By developing the FPGA hardware-based self-adaptive gradient algorithm, high-speed polarization control was implemented. Based on the polarization control unit and properly filtering the raw Gaussian data in terms of their relative phase fluctuation, we implemented a CV QKD over a 50-km fiber channel under strong polarization disturbance. Our results effectively overcome the adverse effect of the rapid fluctuations of the SOP on the CV QKD system, which is one of the major obstacles for wide practical applications of CV QKD in field environments. Future research should focus on optimizing the polarization control technique further to achieve a higher polarization control speed and polarization extinction ratio, which are crucial for the QKD system to withstand harsher environments.

## ACKNOWLEDGMENTS

This work was supported by the National Key R&D Program of China (Grant No. 2016YFA0301403), the National Natural Science Foundation of China (Grants No. 11774209, No. 61378010 and No. 11804208), Key Research and Development Projects of Shanxi Province (Project No. 201803D121065), Applied Basic Research Program of Shanxi Province (Grant No. 201801D221010), and Shanxi Grant No. 1331KSC.

- [1] C. H. Bennett and G. Brassard, in *Proceedings of the IEEE International Conference on Computers, Systems, and Signal Processing, Bangalore, 1984* (IEEE, Piscataway, 1984), pp. 175–179.
- [2] N. Gisin, G. Ribordy, W. Tittel, and H. Zbinden, *Rev. Mod. Phys.* **74**, 145 (2002).
- [3] V. Scarani, H. Bechmann-Pasquinucci, N. J. Cerf, M. Dusek, N. Lütkenhaus, and M. Peev, *Rev. Mod. Phys.* **81**, 1301 (2009).
- [4] C. Weedbrook, S. Pirandola, R. García-Patrón, N. J. Cerf, T. C. Ralph, J. H. Shapiro, and S. Lloyd, *Rev. Mod. Phys.* **84**, 621 (2012).
- [5] H.-K. Lo, M. Curty, and K. Tamaki, *Nat. Photon.* **8**, 595 (2014).
- [6] S. Pirandola, U. L. Andersen, L. Banchi, M. Berta, D. Bunandar, R. Colbeck, D. Englund, T. Gehring, C. Lupo, C. Ottaviani *et al.*, [arXiv:1906.01645](https://arxiv.org/abs/1906.01645).
- [7] E. Diamanti and A. Leverrier, *Entropy* **17**, 6072 (2015).
- [8] F. Grosshans, G. Van Assche, J. Wenger, R. Brouri, N. J. Cerf, and P. Grangier, *Nature (London)* **421**, 238 (2003).
- [9] A. M. Lance, T. Symul, V. Sharma, C. Weedbrook, T. C. Ralph, and P. K. Lam, *Phys. Rev. Lett.* **95**, 180503 (2005).
- [10] B. Qi, L.-L. Huang, L. Qian, and H.-K. Lo, *Phys. Rev. A* **76**, 052323 (2007).

- [11] J. Lodewyck, M. Bloch, R. García-Patrón, S. Fossier, E. Karpov, E. Diamanti, T. Debuisschert, N. J. Cerf, R. Tualle-Brouri, S. W. McLaughlin *et al.*, *Phys. Rev. A* **76**, 042305 (2007).
- [12] R. Filip, *Phys. Rev. A* **77**, 022310 (2008).
- [13] L. S. Madsen, V. C. Usenko, M. Lassen, R. Filip, and U. L. Andersen, *Nat. Commun.* **3**, 1083 (2012).
- [14] P. Jouguet, S. Kunz-Jacques, A. Leverrier, P. Grangier, and E. Diamanti, *Nat. Photon.* **7**, 378 (2013).
- [15] T. Gehring, V. Händchen, J. Duhme, F. Furrer, T. Franz, C. Pacher, R. F. Werner, and R. Schnabel, *Nat. Commun.* **6**, 8795 (2015).
- [16] S. Pirandola, C. Ottaviani, G. Spedalieri, C. Weedbrook, S. L. Braunstein, S. Lloyd, T. Gehring, C. S. Jacobsen, and U. L. Andersen, *Nat. Photon.* **9**, 397 (2015).
- [17] N. Walk, S. Hosseini, J. Geng, O. Thearle, J. Y. Haw, S. Armstrong, S. M. Assad, J. Janousek, T. C. Ralph, T. Symul *et al.*, *Optica* **3**, 634 (2016).
- [18] Y.-M. Li, X.-Y. Wang, Z.-L. Bai, W.-Y. Liu, S.-S. Yang, and K.-C. Peng, *Chin. Phys. B* **26**, 040303 (2017).
- [19] N. Wang, S.-N. Du, W.-Y. Liu, X.-Y. Wang, Y.-M. Li, and K.-C. Peng, *Phys. Rev. Appl.* **10**, 064028 (2018).
- [20] R. Kumar, H. Qin, and R. Alléaume, *New J. Phys.* **17**, 043027 (2015).
- [21] V. C. Usenko and F. Grosshans, *Phys. Rev. A* **92**, 062337 (2015).
- [22] D. Huang, P. Huang, H.-S. Li, T. Wang, Y.-M. Zhou, and G.-H. Zeng, *Opt. Lett.* **41**, 3511 (2016).
- [23] R. Namiki, A. Kitagawa, and T. Hirano, *Phys. Rev. A* **98**, 042319 (2018).
- [24] Y. Guo, W. Ye, H. Zhong, and Q. Liao, *Phys. Rev. A* **99**, 032327 (2019).
- [25] Y.-C. Zhang, Z.-Y. Li, Z.-Y. Chen, C. Weedbrook, Y.-J. Zhao, X.-Y. Wang, Y.-D. Huang, C.-C. Xu, X.-X. Zhang, Z.-Y. Wang *et al.*, *Quantum Sci. Technol.* **4**, 035006 (2019).
- [26] B. Qi, P. G. Evans, and W. P. Grice, *Phys. Rev. A* **97**, 012317 (2018).
- [27] J. Lin, T. Upadhyaya, and N. Lütkenhaus, *Phys. Rev. X* **9**, 041064 (2019).
- [28] S. Ghorai, P. Grangier, E. Diamanti, and A. Leverrier, *Phys. Rev. X* **9**, 021059 (2019).
- [29] G. Zhang, J. Y. Haw, H. Cai, F. Xu, S. M. Assad, J. F. Fitzsimons, X. Zhou, Y. Zhang, S. Yu, J. Wu *et al.*, *Nat. Photon.* **13**, 839 (2019).
- [30] B. Qi, W. Zhu, L. Qian, and H. K. Lo, *New J. Phys.* **12**, 103042 (2010).
- [31] F. Karinou, H. H. Brunner, C.-H. F. Fung, L. C. Comandar, S. Bettelli, D. Hillerkuss, M. Kuschnerov, S. Mikroulis, D. Wang, C. Xie *et al.*, *IEEE Photon. Tech. Lett.* **30**, 650 (2018).
- [32] D. Huang, D. Lin, C. Wang, W. Liu, S. Fang, J. Peng, P. Huang, and G. Zeng, *Opt. Express* **23**, 17511 (2015).
- [33] S. Kleis, J. Steinmayer, R. H. Derksen, and C. G. Schaeffer, *Opt. Express* **27**, 16540 (2019).
- [34] T. A. Eriksson, T. Hirano, B. J. Puttnam, G. Rademacher, R. S. Luis, M. Fujiwara, R. Namiki, Y. Awaji, M. Takeoka, N. Wada *et al.*, *Commun. Phys.* **2**, 9 (2019).
- [35] P. Jouguet, S. Kunz-Jacques, E. Diamanti, and A. Leverrier, *Phys. Rev. A* **86**, 032309 (2012).
- [36] J.-Z. Huang, C. Weedbrook, Z.-Q. Yin, S. Wang, H.-W. Li, W. Chen, G.-C. Guo, and Z.-F. Han, *Phys. Rev. A* **87**, 062329 (2013).
- [37] X.-C. Ma, S.-H. Sun, M.-S. Jiang, and L.-M. Liang, *Phys. Rev. A* **88**, 022339 (2013).
- [38] P. Jouguet, S. Kunz-Jacques, and E. Diamanti, *Phys. Rev. A* **87**, 062313 (2013).
- [39] X.-C. Ma, S.-H. Sun, M.-S. Jiang, and L.-M. Liang, *Phys. Rev. A* **87**, 052309 (2013).
- [40] J.-Z. Huang, S. Kunz-Jacques, P. Jouguet, C. Weedbrook, Z.-Q. Yin, S. Wang, W. Chen, G.-C. Guo, and Z.-F. Han, *Phys. Rev. A* **89**, 032304 (2014).
- [41] E. Diamanti, H.-K. Lo, B. Qi, and Z.-L. Yuan, *npj Quantum Inf.* **2**, 16025 (2016).
- [42] H. Qin, R. Kumar, and R. Alléaume, *Phys. Rev. A* **94**, 012325 (2016).
- [43] W.-Y. Liu, X.-Y. Wang, N. Wang, S.-N. Du, and Y.-M. Li, *Phys. Rev. A* **96**, 042312 (2017).
- [44] I. Derkach, V. C. Usenko, and R. Filip, *Phys. Rev. A* **96**, 062309 (2017).
- [45] Y.-J. Zhao, Y.-C. Zhang, Y.-D. Huang, B.-J. Xu, S. Yu, and H. Guo, *J. Phys. B* **52**, 015501 (2019).
- [46] Y. Zheng, P. Huang, A.-Q. Huang, J.-Y. Peng, and G.-H. Zeng, *Phys. Rev. A* **100**, 012313 (2019).
- [47] F.-H. Xu, X.-F. Ma, Q. Zhang, H.-K. Lo, and J.-W. Pan, *Rev. Mod. Phys.* **92**, 025002 (2020).
- [48] Y. Kidoh, Y. Suematsu, and K. Furuya, *IEEE J. Quantum Electron.* **17**, 991 (1981).
- [49] R. Noé, *Electron. Lett.* **22**, 772 (1986).
- [50] T. Yoshino, M. Yokota, and T. Kenmochi, *Electron. Lett.* **39**, 1800 (2003).
- [51] W.-F. Rong and L. Dupont, *Opt. Commun.* **259**, 603 (2006).
- [52] Y. Zhang, C.-X. Yang, S.-G. Li, H. Yan, J.-C. Yin, C. Gu, and G.-F. Jin, *Opt. Express* **14**, 3484 (2006).
- [53] Z.-Y. Li, C.-Q. Wu, H. Dong, and P. Shum, *Opt. Lett.* **32**, 2900 (2007).
- [54] B. Koch, R. Noé, D. Sandel, and V. Mirvoda, *Opt. Express* **22**, 8259 (2014).
- [55] J. Chen, G. Wu, Y. Li, E. Wu, and H.-P. Zeng, *Opt. Express* **15**, 17928 (2007).
- [56] G. B. Xavier, G. V. de Faria, G. P. Temporão, and J. P. von der Weid, *Opt. Express* **16**, 1867 (2008).
- [57] J. Chen, G. Wu, L. Xu, X. Gu, E. Wu, and H.-P. Zeng, *New J. Phys.* **11**, 065004 (2009).
- [58] G. Xavier, N. Walenta, G. de Faria, G. Temporão, N. Gisin, H. Zbinden, and J. P. von der Weid, *New J. Phys.* **11**, 045015 (2009).
- [59] D.-D. Li, S. Gao, G. C. Li, L. Xue, L. W. Wang, C.-B. Lu, Y. Xiang, Z. Y. Zhao, L. C. Yan, Z.-Y. Chen *et al.*, *Opt. Express* **26**, 22793 (2018).
- [60] Y.-Y. Ding, W. Chen, H. Chen, C. Wang, Y.-P. Li, S. Wang, Z.-Q. Yin, G.-C. Guo, and Z.-F. Han, *Opt. Lett.* **42**, 1023 (2017).
- [61] T. Wang, P. Huang, S.-Y. Wang, and G.-H. Zeng, *Opt. Express* **27**, 26689 (2019).
- [62] X.-Y. Wang, J.-Q. Liu, X. F. Li, and Y.-M. Li, *IEEE J. Quantum Electron.* **51**, 5200206 (2015).
- [63] A. Leverrier, F. Grosshans, and P. Grangier, *Phys. Rev. A* **81**, 062343 (2010).